Investigation on cold start issues of methanol engines and its improvement from the perspective of droplet evaporation

Bo Yuan[1,2&], Huali Zhao[1,2&], Yuhan Huang[3], Miao Zhang[4], Zhihui Song[4], Yuan Shen[4], Xiaobei Cheng[1,2], Zhaowen Wang[1,2*]

[1] School of Energy and Power Engineering, Huazhong University of Science and Technology, Wuhan, 430074, China

[2] State Key Laboratory of Coal Combustion, Huazhong University of Science and Technology, Wuhan, 430074, China

[3] Centre for Green Technology, School of Civil and Environmental Engineering, University of Technology Sydney, NSW 2007, Australia

[4] Geely Royal Engine Components Co., Ltd, Ningbo, 315000, China

* Corresponding author:

Dr. Zhaowen Wang, Email: wangzhaowen1978@163.com, Phone: +86 15827580480

& Co-authors: These authors contributed equally

Abstract

The cold start issue of methanol engines limits their wide application in cold seasons and regions. To explore the underlying mechanisms and propose effective improvement measures, the evaporation characteristics of methanol at 243-303 K were first investigated by the single droplet method in this study. The effects of ambient temperature, initial diameter, fuel temperature and intake air flow velocity on evaporation of methanol droplets were quantitatively analyzed and their guidance for improving the cold start performance of methanol engines were discussed. The results revealed that the evaporation process of methanol droplets in low temperature and humid environment showed two-stage feature due to its hygroscopicity, including pure methanol evaporation and water-dominated evaporation of methanol-water mixture, but it could be regarded as the evaporation of a pseudo single component and the same was true for other binary mixtures. The existence of water in methanol droplets not only led to their incomplete evaporation at temperatures below 263 K, but also caused the linear change of their evaporation rates with temperature, which was different from the exponential change of pure methanol evaporation rate with temperature. Increasing the ambient temperature from 243-283 K to 293 K was optimal for promoting methanol evaporation. Reducing droplet diameter inhibited the water absorption of methanol droplets, thus enhancing their evaporation rates. Increasing fuel temperature could not promote droplet evaporation, but mainly influenced water absorption of methanol droplets. The promotion effect of air flow on methanol evaporation became weaker with the increase of intake air flow velocity, especially when it exceeded 3 m/s. The findings

of this study suggest that multiple methods should be combined to improve the cold start performance of methanol engines.

Keywords: Cold start issues; Droplet evaporation; Low temperature; Initial diameter; Fuel temperature; Intake air flow velocity

Highlights

- Methanol droplets could not completely evaporate at temperatures below 263 K due to its hygroscopicity.
- Raising ambient temperature from 243-283 K to 293 K was optimal for promoting evaporation.
- The evaporation of binary mixtures could be regarded as the evaporation of a pseudo single component.
- The water absorption of methanol droplets was inhibited by reducing droplet diameter.
- Increasing fuel temperature could not promote droplet evaporation.

Graphical abstract

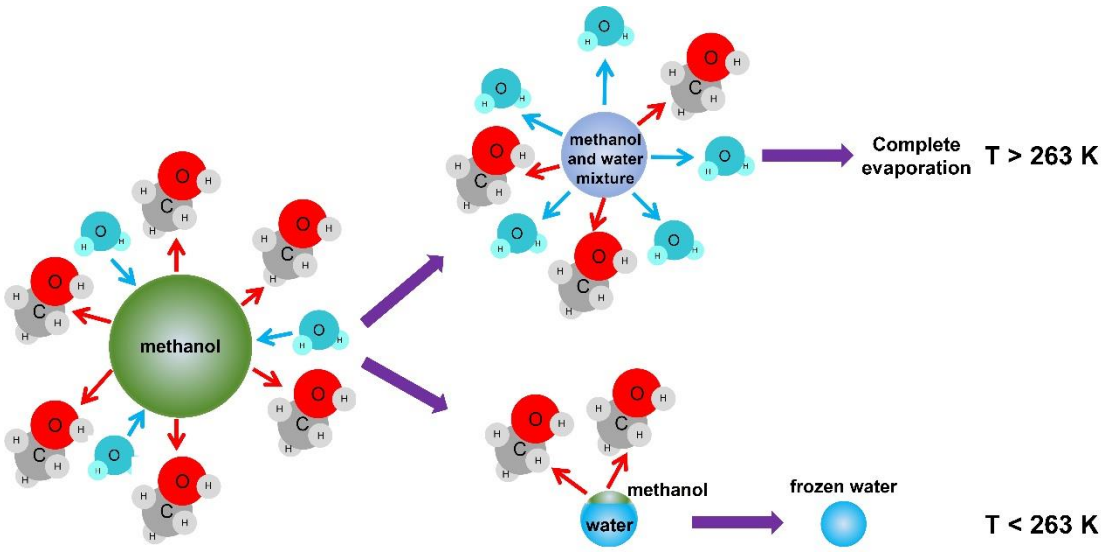

Nomenclature

Abbreviations

PM	Particulate matters	BMEP	Brake mean effective pressure
NO_x	Nitrogen oxides	BTE	Brake thermal efficiency
UHC	Unburned hydrocarbons	BSFC	Brake specific fuel consumption
CO_2	Carbon dioxides	IMEP	Indicated mean effective pressure
CO	Carbon monoxide	CVC	Constant volume chamber
SI	Spark ignition		

Symbols

d	droplet diameter
d_0	initial droplet diameter
d_1	droplet diameter when evaporation is completed
σ	normalized squared diameter when evaporation is completed
τ_1	time of the first stage
τ_2	time of the second stage
τ_i	ideal normalized droplet lifetime
τ_a	actual normalized droplet lifetime
t_i	ideal droplet lifetime
t_a	actual droplet lifetime
K_1	average evaporation rate of the first stage
K_2	average evaporation rate of the second stage

K_a average evaporation rate of methanol droplets

K_w average evaporation rate of water droplets

K_c calculated value of average evaporation rate of methanol droplets

K_p evaporation rate constant of the pseudo single component

P_1 proportion of the first stage

P_2 proportion of the second stage

P_{K1} improved percent of K_1

P_{K2} improved percent of K_2

P_{Ka} improved percent of K_a

P_τ increased percent from τ_i to τ_a

$P_{\tau i}$ relative change (increased percent or decreased percent) of τ_i

$P_{\tau a}$ relative change (increased percent or decreased percent) of τ_a

η_{K1} improvement efficiency of K_1

η_{K2} improvement efficiency of K_2

η_{Ka} improvement efficiency of K_a

ΔT Value of increased ambient temperature

$\Delta T'$ Value of increased fuel temperature

V intake air flow velocity

T_d droplet temperature

RH relative humidity

AH absolute humidity

1 Introduction

Automobiles are still predominately powered by traditional hydrocarbon fuels nowadays, inevitably leading to significant harmful pollutants such as particulate matters (PM), nitrogen oxides (NO_x) and unburned hydrocarbons (UHC) [1]. Further, the production of carbon dioxides (CO_2) also exacerbates the greenhouse effect [2]. The urgent need to achieve the carbon neutralization goal drives the engine industry to search for green, low-carbon and renewable alternative fuels [3]. Methanol has received extensive attention due to its unique advantages [4]. On the one hand, methanol can be produced by both fossil fuels (e.g., coal, biomass, natural gas and coke oven gas [5]) and the synthesis of CO_2 captured in the air and hydrogen obtained by electrolysis of water from renewable energies [6], so as to realize the green cycle of CO_2 to fuel. On the other hand, methanol has a high flame speed [7], and its low C/H ratio produces less CO_2 than gasoline. The high oxygen content reduces the formation of carbon monoxide (CO) [8]. The high latent heat of vaporization and more ternary molecules in the combustion products lead to lower in-cylinder temperature [9], not only reducing NO_x emissions and heat loss, but also providing better anti-knock performance [10]. The high-octane number allows higher compression ratios [11], thereby improving engine thermal efficiency [12]. Furthermore, methanol is liquid at standard temperature and pressure [13], making it easier to store and transport [14].

Many scholars have studied the performance of methanol-fueled engines. Xu et al. [15] experimentally and numerically studied the engine performance and emission characteristics of methanol and iso-octane in a heavy-duty direct-injection compression

ignition engine operating in partially premixed combustion (PPC) regimes. The results showed that the lower CO and NO_x emissions as well as much higher combustion efficiency with a similar power output were achieved for methanol as compared to iso-octane. Celik et al. [16] comparatively investigated the performance and emission characteristics of methanol and gasoline in a single-cylinder engine at different compression ratios. They found that methanol produced less CO, CO_2 and NO_x emissions than gasoline at compression ratio of 6, with insignificant loss of power. Knock occurred in gasoline mode but not in methanol mode when the compression ratio increased from 6 to 10. The power and brake thermal efficiency increased by 14% and 36%, respectively, while the CO, CO_2 and NO_x emissions decreased by 37%, 30% and 22%, respectively. Balki et al. [17] studied the effects of compression ratio on the performance of a single-cylinder low-power spark ignition (SI) engine fueled with pure methanol and unleaded gasoline. The results showed that methanol had higher brake mean effective pressure (BMEP), cylinder pressure, brake thermal efficiency (BTE) and brake specific fuel consumption (BSFC), and lower UHC, CO and NO_x emissions than that of gasoline at compression ratios of 8.5-9.5. When the compression ratio increased from 8.0 to 8.5, the BMEP, BTE and BSFC of methanol increased by 10.5%, 4.5% and 30.2% respectively. Zhu et al. [18] studied the performance of a pure methanol engine modified from a multi-cylinder port fuel injection SI heavy-duty natural gas engine. The results showed that the pure methanol engine reached a peak BTE of 41.4%, which was 3% higher than the original natural gas engine. NO_x and CO emissions were reduced, while UHC emissions were increased. Meanwhile, the

coefficient of variation of the indicated mean effective pressure (IMEP) remained below 2% at EGR rate of 31%. In summary, the above studies showed that methanol engines have great advantages in energy saving and emission reduction. Combined with green production, methanol engines have broad application prospects.

However, methanol evaporates slowly at low ambient temperatures due to its low vapor pressure and high latent heat of vaporization [10], resulting in cold start issues of methanol engines. Li et al. [19] concluded that methanol engines cannot start reliably without auxiliary devices under an ambient temperature below 289 K even when a large amount of methanol is injected, which limits the use of methanol engines in cold seasons and regions. Therefore, to promote the application of methanol engines, it is of great significance to explore the evaporation characteristics of methanol at low temperatures and find ways to improve its evaporation rate.

In real engines, the fuel is injected into combustion chamber through high pressure injectors and evaporates in the form of spray droplets to produce an ignitable mixture before combustion and power output [20]. As a result, the engine performance is closely related to the evaporation of droplets. Thus, it is a common and necessary method to investigate the fuel evaporation characteristics from the perspective of a single droplet [21]. Many scholars have used this method to study the evaporation characteristics of methanol fuel. Yuan et al. [22] studied the evaporation characteristics of methanol droplets at ambient temperatures of 323-473 K. They found that methanol droplets evaporated linearly when the ambient temperature was higher than 373 K, while the evaporation process of methanol droplets was divided into two linear evaporation

125 stages at temperatures below 373 K, which was caused by the hygroscopicity of
126 methanol. Wang et al. [23] studied the evaporation characteristics of methanol droplets
127 at ambient temperatures of 473-1087 K and reported a similar conclusion: the
128 normalized square diameter of methanol droplets decreased linearly with time. The
129 evaporation of methanol droplets in different humidity environments at an ambient
130 temperature of 297 K was investigated by Law [24]. The results showed that methanol
131 droplets evaporated linearly when the humidity was 0%. As the humidity increased, the
132 droplet normalized diameter curve became a downwards concave and the droplet
133 lifetime prolonged. Hegseth et al. [25] studied the evaporation characteristics of
134 methanol droplets at an atmospheric pressure and an ambient temperature of 293 K.
135 They found a convection driven by surface tension gradient inside the droplets during
136 evaporation. Kosasih et al. [26] investigated the heat and mass transfer of methanol
137 droplets at ambient temperatures of 308-328 K and air flow rates of 0.1-0.7 m/s.

138 However, the ambient temperatures in above studies were all over 293 K. There is
139 a research gap in the evaporation of methanol droplets at temperatures below 293 K,
140 which is of great significance for the cold start of methanol engines. Depending on the
141 seasons and regions, the start-up temperature of an engine usually changes between 243
142 and 303 K. Therefore, this study investigated the evaporation characteristics of
143 methanol droplets at a wide range of ambient temperatures between 243-303 K. The
144 effects of ambient temperature, initial droplet diameter, fuel temperature and intake air
145 flow velocity on the evaporation of methanol droplets were quantitatively analyzed,
146 and their implications for designing methanol engines were discussed. The findings of

147 this research are expected to provide great theoretical and practical guidance for
148 tackling the cold start issues of methanol engines and thus promote their applications
149 in cold seasons and regions.
150

151 # 2 Material and methods

152 ## 2.1 Experimental setup

153 **Fig. 1** shows the schematic of the experimental setup for the evaporation of
154 methanol droplets at low temperatures. It consisted of a droplet generation and transport
155 system, a temperature control system, a fuel heating system, an inlet air flow system
156 and an image acquisition system. In the droplet generation and transport system, as the
157 stepper motor I runs, a given volume of liquid was squeezed out by a microliter syringe
158 and then a droplet with the specific diameter was formed on the K-type thermocouple
159 with the diameter of 0.08 mm, which was sent to the constant volume chamber (CVC)
160 by stepper motor III. According to the conclusion of Rehman et al. [27], the effect of
161 thermocouple was ignorable when the ratio of the square of thermocouple diameter to
162 the square of initial droplet diameter was less than 0.01. Considering that the diameter
163 of the thermocouple was 0.08 mm and the diameters of the droplets in the experiment
164 exceeded 0.8 mm, the effect of heat conduction by thermocouple on droplet evaporation
165 could be negligible. The temperature control was achieved by the environmental
166 chamber which could change between 233 and 353 K. Three K-type thermocouples
167 were evenly arranged in the CVC to ensure uniform ambient temperature. The accuracy
168 of temperature control was ±1 K. The fuel heating system was used to change the

169 methanol temperature before the evaporation, which was reached by the heating plate
170 pasted on the baffle below the droplet. Since the heating plate was exposed to the cold
171 environment, a large amount of heat generated by the heating plate was dissipated to
172 the environment and only a small part of the heat was used to improve the fuel
173 temperature, which ultimately led to a smaller increase in fuel temperature. The
174 maximum value of increased fuel temperature was only 8.5 K in this experiment. After
175 the baffle was removed by the stepper motor II, the droplets with different fuel
176 temperatures were sent to the CVC. The inlet air flow system mainly included an intake
177 port manufactured by three-dimensional printing, a flowmeter (1.5% accuracy) and a
178 blower, which could vary the intake air flow velocity. In the image acquisition system,
179 a LED lamp, an industrial camera (MV-CS060-10GM) and a tele-macro lens (Nikon
180 Micro-ED 200 mm f/4) were combined to get the droplet images with the resolution of
181 1072×1548 pixels. Due to the slow evaporation of methanol droplets at low
182 temperatures, the sampling frequency was changed between 1 and 18 frames per second
183 (fps).

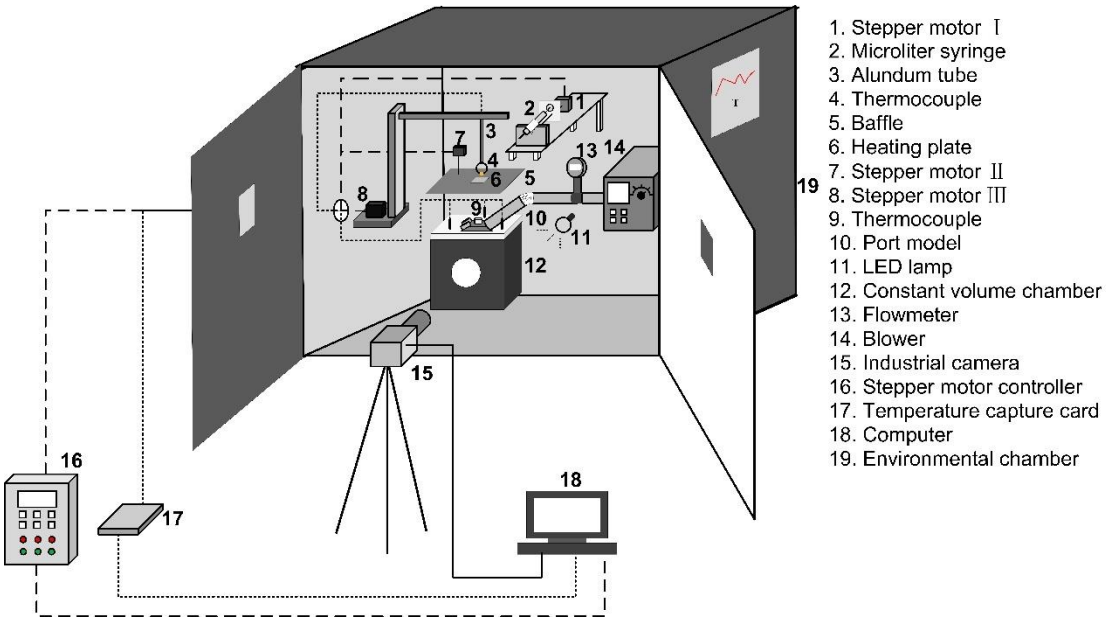

Fig. 1. The schematic of experimental setup

2.2 Test conditions

The evaporation characteristics of methanol droplets with various initial diameters were first investigated at ambient temperatures of 243-303 K. Then the fuel temperature and intake air flow velocity were increased to study their promotion effects on the evaporation of methanol droplets at 273 K. The specific experimental conditions were presented in **Table 1**.

Table 1 Experimental conditions for droplet evaporation.

Ambient pressure (atm)	1
Ambient temperature (K)	243-303
Initial diameter (mm)	0.816-1.604
Value of increased fuel temperature (K)	0-8.5
Intake air flow velocity (m/s)	0-3.20

2.3 Data processing

Droplet diameter was a key parameter in the evaporation process, which was obtained by a MATLAB code. The procedures of image processing were shown in **Fig. 2**. Firstly, a region of 300*300 with the droplet at the center was cut out from the raw image (1072*1548). Secondly, the image was binarized by a proper threshold. Then thermocouple wire on both sides of the droplet was removed. Finally, the droplet boundary was extracted from the image and the pixel number (N) of the droplet was obtained. The droplet diameter (d) was calculated by Eq. (1) where l was the image spatial resolution:

$$d = \sqrt{\frac{4*N*(\frac{1}{l})^2}{\pi}} \quad (1)$$

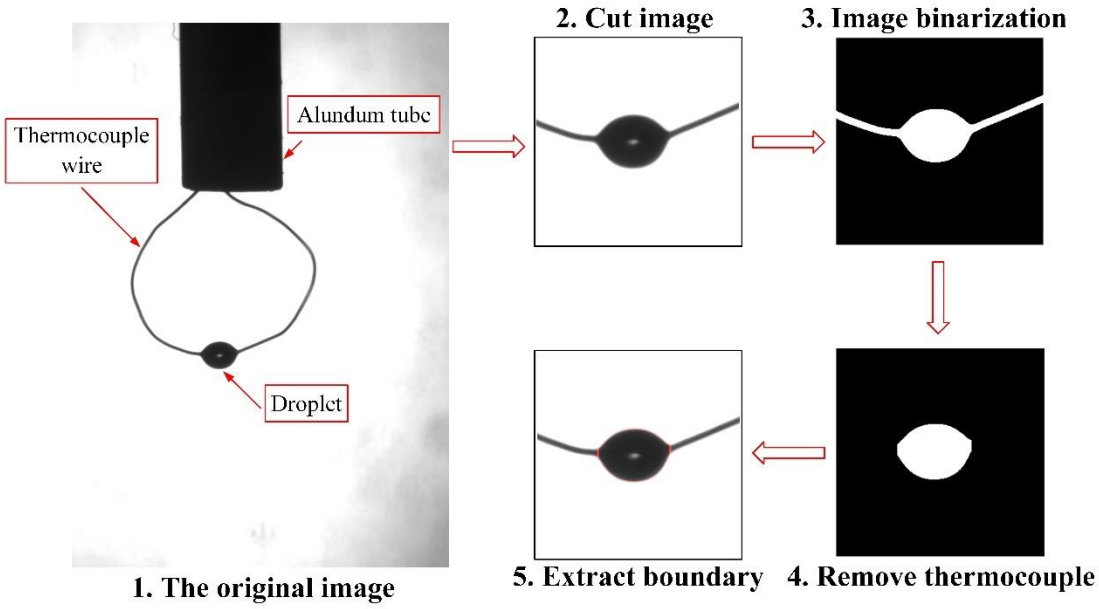

Fig. 2. The procedures of image processing.

Droplet lifetime and evaporation rate were also significant parameters to evaluate the evaporation, which were described in **Fig. 3**. The evaporation process of methanol droplets included two linear stages and the demarcation point between them was

determined by the maximum value of the second derivative of the concave part of droplet diameter curve. The average evaporation rates of the first and second stages were defined as K_1 and K_2, respectively which were obtained by linear fitting for each stage. The times of two stages were defined as τ_1 and τ_2, respectively, and their sum was the actual normalized lifetime τ_a. The ideal normalized lifetime, τ_i, was defined by Eq. (2), where σ was the corresponding normalized squared diameter at the end of evaporation, which represented the lifetime of methanol droplets without the disturbance of water vapor. The difference between τ_a and τ_i indicated the effect of water vapor on the evaporation of methanol droplets. In addition, the average evaporation rate of methanol droplets in the entire evaporation process, K_a, was calculated by the Eq. (3), where d_0 was the initial droplet diameter, d_1 was the droplet diameter when the evaporation was completed and t was the evaporation time.

$$\tau_i = (1-\sigma)/K_1 \tag{2}$$

$$K_a = (d_0^2 - d_1^2)/t \tag{3}$$

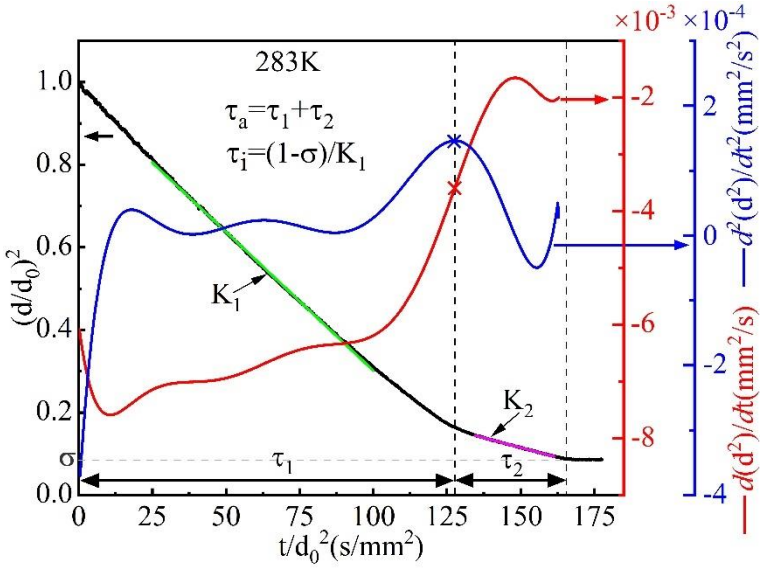

Fig. 3. The parameters characterizing the evaporation of methanol droplets.

2.4 Experimental errors and uncertainties

The errors of droplet characteristic parameters were mainly caused by the random error of experiment and the error of droplet boundary identification. Experiment was repeated five times to minimize the random error (δ) which was calculated by Eq. (4):

$$\delta = \sqrt{(x_1 - \bar{x})^2 + ((x_2 - \bar{x})^2) + \cdots + ((x_n - \bar{x})^2)/(n-1)} \quad (4)$$

where x_1、$x_2 \cdots x_n$ were the values of repeated experiments, $\bar{x}$ was the average value, and *n* was the number of experiment.

Regarding the error of droplet boundary identification, if the experimental result *R* satisfied Eq. (5) [28], [29] [30], the relative uncertainty of *R* was calculated by Eq. (6):

$$R = Y_1^{a_1} * Y_2^{a_2} * \cdots * Y_n^{a_n} \quad (5)$$

$$\frac{\Delta R}{R} = \sqrt{(a_1 * \frac{\Delta Y_1}{Y_1})^2 + (a_2 * \frac{\Delta Y_2}{Y_2})^2 + \cdots + (a_n * \frac{\Delta Y_n}{Y_n})^2} \quad (6)$$

where Y_i was the variable, and ΔR and ΔY_i were the uncertainties of *R* and Y_i, respectively. Assuming that a pixel was a square, then the droplet area could be calculated by Eq. (7) where *L* was the side length of pixel, D_0 was the diameter of alundum tube for calibration, *M* was the pixel number of alundum tube diameter, and *N* was the pixel number of the droplet.

$$S = L^2 * N = \left(\frac{D_0}{M}\right)^2 * N = D_0^2 * M^{-2} * N \quad (7)$$

Assuming that the droplet was a sphere, then the relative uncertainty of square of droplet diameter could be calculated by Eq. (8) where ΔN, ΔD_0 and ΔM were the uncertainties of the pixel number of the droplet, the diameter and pixel number of

alundum tube, respectively. In this study, the droplet diameter varied from 0.816 mm to 1.604 mm and D_0 was 2.5 mm (measured by a vernier caliper whose accuracy was 0.02 mm, so ΔD_0 was 0.02 mm). It was assumed that there was an error of two pixels when measuring alundum tube diameter, so ΔM was 2. According to Morin et al. [31], the pixels on the droplet boundary were regarded as errors. For the droplet with diameter of 0.816 mm, M, N and ΔN were 290, 6512 and 260, respectively, so $\Delta D^2/ D^2$ was 4.52%. For the droplet with diameter of 1.604 mm, M, N and ΔN were 290, 25149 and 562, respectively, so $\Delta D^2/ D^2$ was 3.08%. Overall, it could be concluded that the uncertainty of the droplet diameter was less than 5%.

$$\frac{\Delta D^2}{D^2} = \frac{\Delta S}{S} = \sqrt{(2 * \frac{\Delta D_0}{D_0})^2 + (-2 * \frac{\Delta M}{M})^2 + (\frac{\Delta N}{N})^2} \quad (8)$$

3. Results and discussion

3.1 Evaporation characteristics of methanol droplets at low temperatures

Fig. 4(a) plots the normalized squared diameters and temperatures of methanol droplets at temperatures of 243-303 K. The droplet diameter and the time are normalized to eliminate the effect of different initial diameters between repeated experiments caused by surface tension [32]. As shown in **Fig. 4(a),** the evaporation process of methanol droplets at 253-303 K is divided into two stages by the two linear parts of the diameter curves and the two quasi-steady parts of the droplet temperature curves, which is similar to the evaporation of binary mixture. It is because the first stage is the evaporation of pure methanol and the second stage is the water-dominated evaporation of methanol-water mixture [33]. The d^2 law is obeyed in each stage, which

is consistent with the evaporation of methanol droplets at ambient temperature of 323-373 K [22]. This is also the result of the hygroscopicity of methanol in humid environment, because there is always water vapor in the air even when the ambient temperature is extremely low. The normalized squared diameter corresponding to the turning point between the first and second stages gradually decreases with the decrease of ambient temperature, which suggests that more methanol is evaporated in the first stage and the concentration of water in the mixture is increased. The reason is that less water vapor is absorbed by the methanol droplets, which is attributed to the reduction of number of water molecule in the environment caused by the lower saturation vapor pressure and slower evaporation of water. **Fig. 4(b)** describes the relative humidity and absolute humidity at various temperatures. It can be seen from **Fig. 4(b)** that the relative humidity is gradually reduced when ambient temperature increases, which is due to the simultaneous increase of the partial pressure and saturation vapor pressure of water vapor in the air. To better evaluate the content of water vapor in the air, absolute humidity is used to represent the mass of water vapor per unit volume of air. According to **Fig. 4(b)**, absolute humidity increases with temperature and reaches the maximum value of 3.76 g/m^3 at 303 K, which is far less than the absolute humidity at temperature of 298 K and relative humidity of 50%. This proves that the content of water vapor in the air is low and its increase is limited when ambient temperature increases from 243 K to 303 K, leading to the little change of turning point between the first and second stages. Owing to the relatively low humidity, the droplets are evaporated by over 85 % in the first stage. Surprisingly, the absorbed water can still evaporate at 263 K when it

is mixed with methanol. Maybe it is the result of the hydrogen bonding interaction between the hydroxyl of methanol and water [34], which promotes the water evaporation. However, the methanol droplets cannot completely evaporate at 253 K, and even the second stage is missing at 243 K, as presented in **Fig. 4(a)**. The experimental images show that the absorbed water is attached on the thermocouple and basically not evaporated. This is due to the separation of methanol and water caused by the low temperature and reduced concentration of methanol in the mixture, and the residual methanol continues to evaporate, while the water freezes on the thermocouple. Then the schematic of evaporation for methanol droplets is concluded in **Fig. 4(c)**. It can be inferred that the freezing phenomenon of water can also occur on the wall once the spray impinges on the engine wall in the cold start process of methanol engines, whose effect on engine performance is needed to consider. With the decrease of ambient temperature, the difference in the droplet diameter curves is more obvious, which implies the slower evaporation of methanol at lower temperatures.

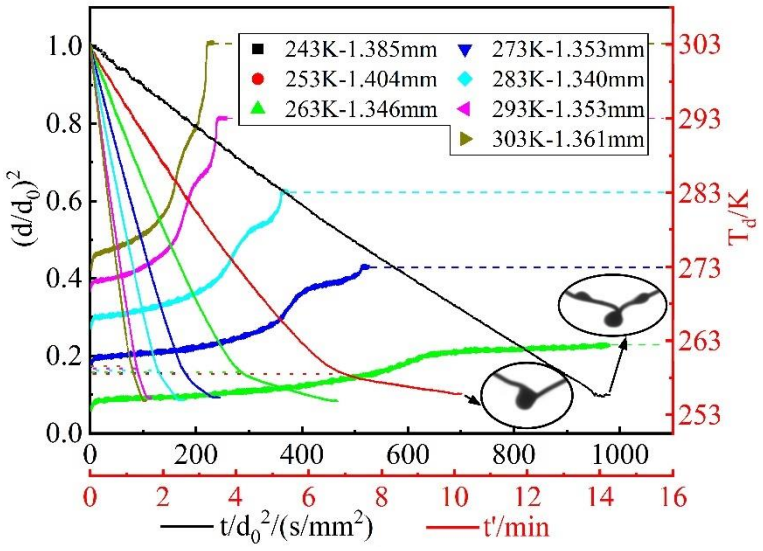

(a)

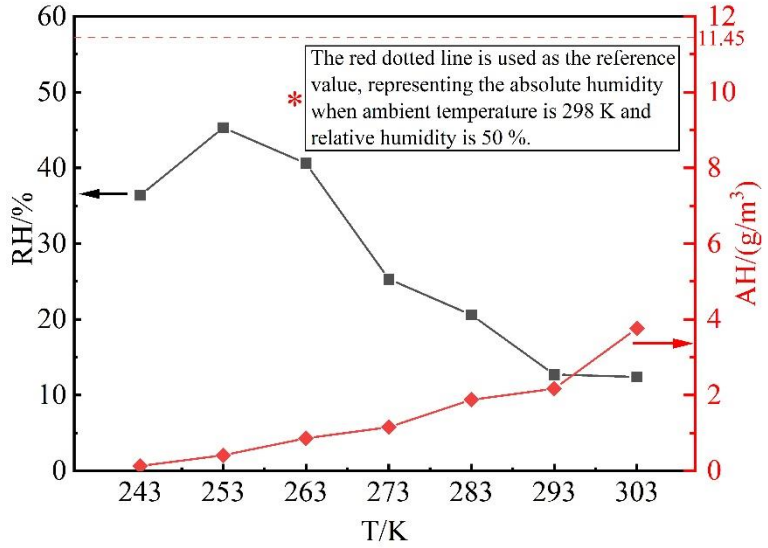

(b)

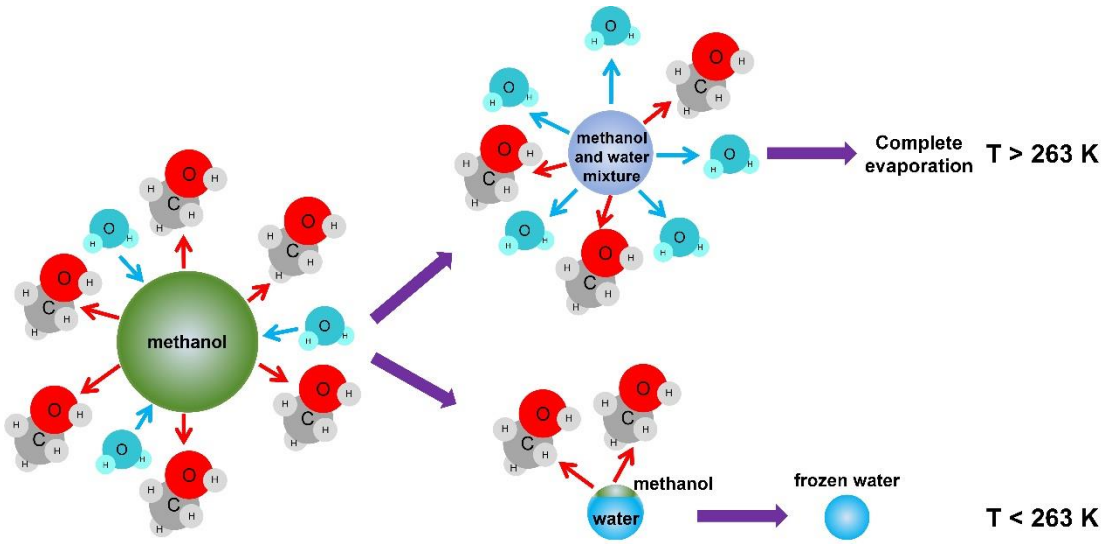

(c)

Fig. 4. (a) Temporal evolution of the normalized squared diameters $(d/d_0)^2$ and temperatures (T_d) of methanol droplets at temperatures of 243-303 K. (b) The change of the relative humidity (RH) and absolute humidity (AH) with ambient temperature. (c) The schematic of evaporation for methanol droplets.

The average evaporation rates of the first and second stages, methanol droplets and pure water at various ambient temperatures, K_1, K_2, K_a and K_w are shown in **Fig. 5**. Apparently, the trends of K_1, K_2 and K_w are similar, that is, the average evaporation

rate varies exponentially with the ambient temperature, while K_a increases linearly with the increase of ambient temperature. Then the empirical formulas for droplet evaporation of single component and binary mixture at low temperatures can be inferred: $K = A * \exp(-T/B) + C$ and $K = A * T + B$, respectively, where K is the average evaporation rate, T is ambient temperature, A, B and C are both constant, which is significant for droplet evaporation simulation. Meanwhile, another method calculating the average evaporation rate of methanol droplets is proposed: $K_c = K_1 * P_1 + K_2 * P_2$, where K_c is the calculated value of the average evaporation rate of methanol droplets, P_1 and P_2 are the proportion of the first and second stages, respectively. The comparison of K_c and K_a is shown in **Fig. 5**. It is found that K_c is in good agreement with K_a, which verifies the accuracy of the proposed method. And this method can also be used for binary mixture evaporation due to the same two-stage feature of the evaporation process. On the other hand, the reduction from K_1 to K_2 is noticeable (more than 64%), especially at temperature below 273 K, resulting in K_a being less than K_1. It can be deduced that the addition of water slows down the evaporation of methanol, while methanol accelerates the water evaporation. Furthermore, K_2 is always larger than K_w, which proves that the second stage is the water-dominated evaporation of methanol-water mixture rather than the evaporation of pure water. The reduced difference between K_2 and K_w is observed with the decrease of temperature. This is due to the increase of water concentration in the methanol-water mixture at lower temperatures.

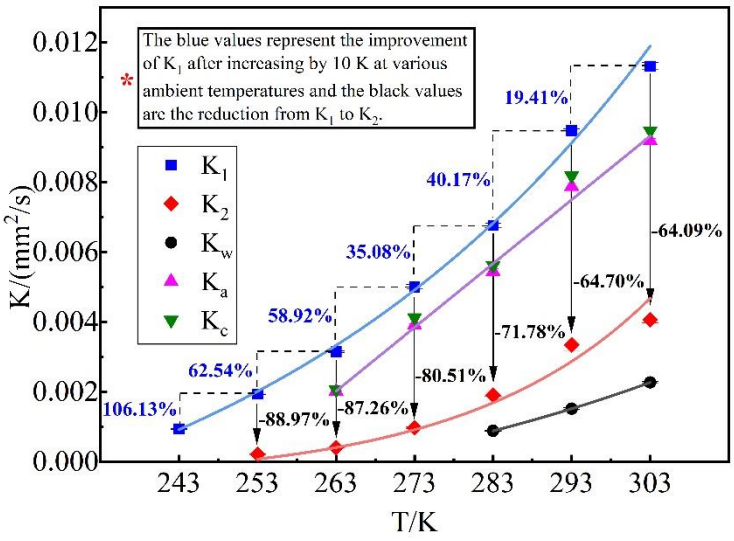

340

341 **Fig. 5.** Variation of the average evaporation rates of the first and second stages (K_1

342 and K_2), methanol droplets (K_a) and pure water (K_w) with ambient temperature. K_c is

343 the calculated value of K_a by another method.

344 In the actual methanol engines, the larger injection quantity and higher latent heat

345 of vaporization of methanol as compared to gasoline can reduce the combustion

346 chamber temperature [10]. This reduces the evaporation rate of methanol, which is the

347 main reason for the cold start difficulty of methanol engines. Therefore, the promotion

348 of methanol evaporation brought by increasing temperature at different initial ambient

349 temperatures is quantitively analyzed. **Fig. 6(a)** illustrates that the improved percent

350 of the average evaporation rates of the first and second stages and methanol droplets,

351 P_{K1}, P_{K2} and P_{Ka}, both increases with the increased temperature ΔT for each initial

352 ambient temperature, but gradually weakens at higher initial ambient temperature. For

353 instance, P_{K1} is 106.13% at an initial temperature of 243 K, but only 19.41% at an

354 initial temperature of 293 K when ΔT is 10 K, as demonstrated in **Fig. 5**. On the other

355 hand, the improvement efficiency of the average evaporation rates of the first and

second stages and methanol droplets, η_{K1}, η_{K2} and η_{Ka}, are defined in **Fig. 6(b)** to evaluate the benefit of increasing ambient temperature on promoting the evaporation of methanol droplets. It can be observed that both of them are decreased with the increase of initial ambient temperature, and first increase and then decrease with ΔT at each initial ambient temperature. There is a maximum value marked with '*' in **Fig. 6(b)**, at which the improvement of evaporation rate brought by an increased temperature of 1 K is maximum. The corresponding ΔT is 50, 40, 30, 20, 10 K for initial ambient temperatures of 243-283 K, respectively. Interestingly, the corresponding actual temperatures are both 293 K. This means that increasing the ambient temperature from original of 243-283 K to 293 K in the cold start process is the way to maximize the benefit of promoting the evaporation by increasing ambient temperature for methanol engines.

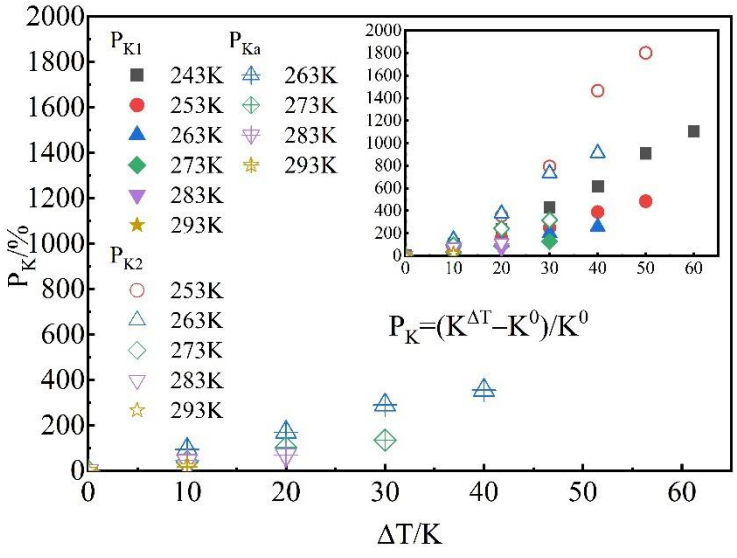

(a)

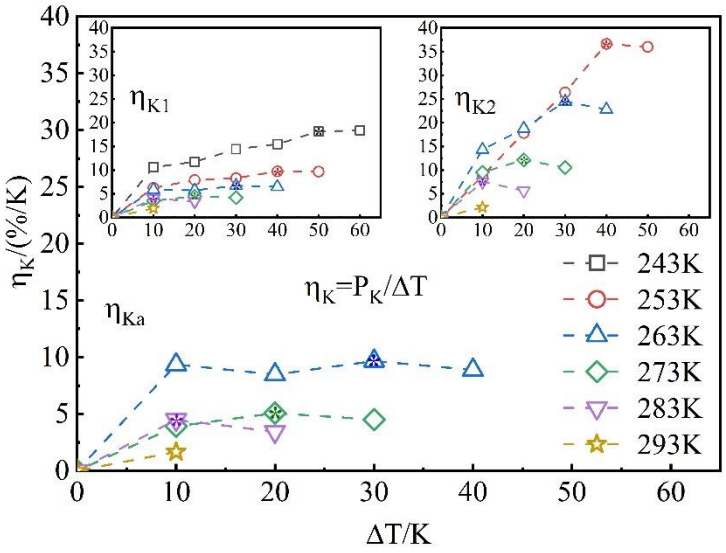

(b)

Fig. 6. (a) Variation of the improved percent (P_{K1}, P_{K2} and P_{Ka}) of K_1, K_2 and K_a with the increased temperature ΔT. $K^{\Delta T}$ is the K after the ambient temperature increases by ΔT and K^0 is the K at initial ambient temperature. (b) Variation of the improvement efficiency (η_{K1}, η_{K2} and η_{Ka}) of K_1, K_2 and K_a with the increased temperature ΔT.

Fig. 7 shows the ideal and actual normalized lifetimes, the time of the first and second stages, and their proportion in the entire lifetime. With the increase of ambient temperature, the ideal and actual normalized lifetimes both decrease exponentially and the latter is always greater than the former due to the presence of the second stage caused by water vapor in the environment. The difference between them is related to the ambient temperature and humidity. As shown in **Fig. 7**, the increased percent from the ideal to the actual normalized lifetime, P_τ, has little change at 283-303 K due to similar low humidity, but rise quickly due to the extremely slow evaporation of methanol-water mixture in the second stage when the ambient temperature is below 273 K. This can be also proved by the rapidly increased proportion of the second stage with

a value of 39.62% at 263 K. Since the methanol droplets cannot completely evaporate at 253 and 243 K owing to the freezing of absorbed water, their lifetimes and the time of the first and second stages are missing.

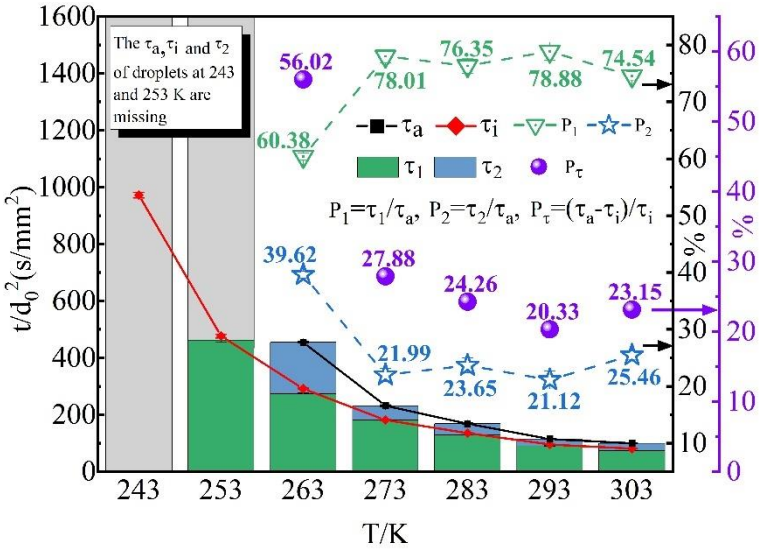

Fig. 7. Variations of the ideal and actual droplet normalized lifetimes (τ_i and τ_a), times of the first and second stages (τ_1 and τ_2), proportion of the first and second stages (P_1 and P_2), and the increased percent of lifetime (P_τ) with ambient temperature.

3.2 Effect of initial droplet diameter on methanol evaporation

With the decrease of ambient temperature, the size of spray droplets in methanol engines become larger [35], which affects the evaporation of methanol droplets and further the cold start performance. Hence, the effect of initial droplet diameter on the evaporation characteristics of methanol droplets is discussed in this section. **Fig. 8** shows temporal evolution of the normalized squared diameters of methanol droplets with different initial diameters at temperatures of 243-303 K. It is noticed that the pure methanol evaporation of the first stage of methanol droplets has weak dependence on

initial droplet diameter. According to the conclusion of Verwey and Birouk [36], the droplet evaporation in quiescent environment is related to molecular diffusion and natural convection. The former is determined by fuel volatility and mainly affected by vapor concentration gradient on the droplet surface, while the latter is proportional to the square of pressure and the cube of droplet diameter. For high volatile droplets, such as methanol, the relative importance of the molecular diffusion appears to govern the entire evaporation process at low temperatures and atmospheric pressure as compared to natural convection, leading to the little effect of initial droplet diameter on pure methanol evaporation. Similarly, Verwey and Birouk [37] also found that the change of the evaporation rate of n-heptane with initial droplet size in quiescent environment at room temperature and atmospheric pressure is insignificant due to its high volatility. However, the effect of initial droplet diameter on the methanol-water mixture evaporation of the second stage is more obvious as compared to the first stage.

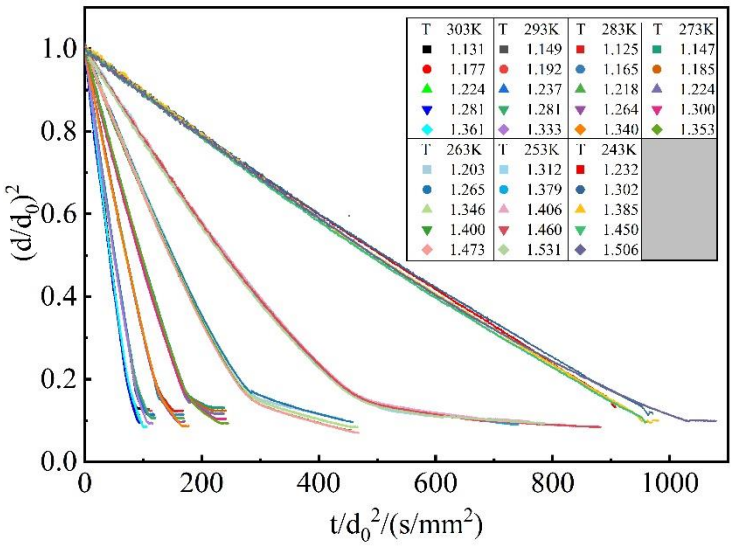

Fig. 8. Temporal evolution of the normalized squared diameters $(d/d_0)^2$ of methanol droplets with different initial diameters at temperature of 243-303 K.

Fig. 9 demonstrates the average evaporation rates of the first and second stages and methanol droplets with various initial diameters at 243-303 K, K_1, K_2 and K_a. As demonstrated in **Fig. 9**, K_1 is almost a constant and do not change with the initial droplet diameter, while K_2 shows relatively large fluctuation, especially at 293 and 303 K. And K_a also shows a different trend, which decreases with the increase of the initial droplet diameter. This can be explained by the fact that the larger the methanol droplet, the more water vapor it absorbs, and the longer time of the second stage is, which can be validated by the increased proportion of the second stage in **Fig. 10(a)**. Then the lifetime of methanol droplets is prolonged and K_a is reduced.

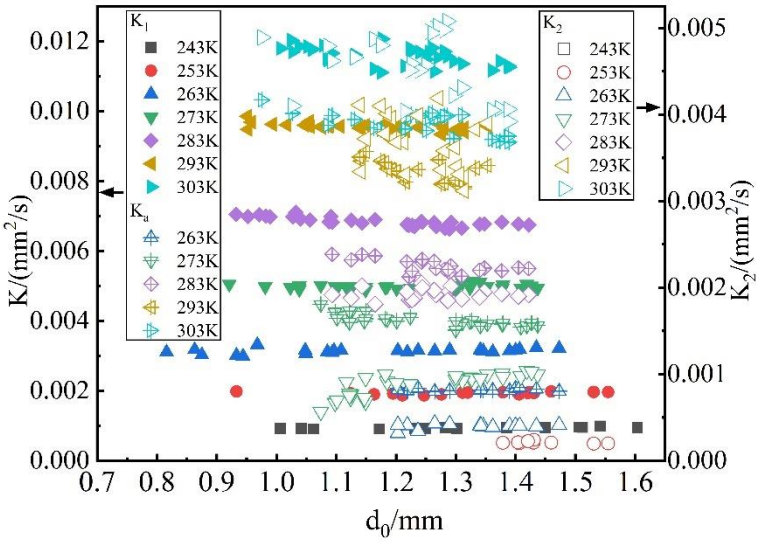

Fig. 9. Variation of the average evaporation rates of the first and second stages (K_1 and K_2) and methanol droplets (K_a) with initial droplet diameter at ambient temperatures of 243-303 K.

Fig. 10(a) shows the evolution of ideal and actual lifetimes with the square of initial droplet diameter at 243-303 K. As presented in **Fig. 10(a)**, the ideal lifetime of methanol droplets without the disturbance of water vapor increases linearly with the

increase of the square of droplet diameter. And the relation between droplet lifetime t and square of droplet diameter d_0^2 is obtained: $t = A * d_0^2$. According to the classical d^2 law of single component evaporation: $d^2 = d_0^2 - K * t$, where K is evaporation rate constant, A is 1/K. Notably, the same trend occurs in the actual lifetime. This suggests that the actual two-stage and binary component evaporation process of methanol droplets can be regarded as the evaporation of a pseudo single component, whose evaporation rate constant can be acquired by the reciprocal of the linear fitting slope of actual lifetime curves, that is, $K_p = 1/A$, where K_p is the evaporation rate constant of the pseudo single component. The variation of K_p with ambient temperature is shown in **Fig. 10(b)**. It can be found that K_p increases linearly rather than exponentially with the increase of ambient temperature, meaning that the pseudo single component is various at each ambient temperature. Base on the above analysis, the lifetime of methanol droplets will be n^2 times of the original if the initial droplet diameter increases by n times. Due to the larger size of spray droplet during the cold start process of methanol engines, the evaporation of methanol droplets is greatly prolonged, resulting in less combustible mixture of methanol vapor and air in a short time, whose combustion is not enough to start the engine. Therefore, in order to enhance the average evaporation rate of methanol droplets and shorten the entire evaporation time of methanol, the size of spray droplets in the cold start process of methanol engines should be reduced by improving injection pressure or other methods. For example, when the droplet diameter is reduced by half, the droplet lifetime can be reduced to 1/4 of the original according to the above formula, which greatly promotes the complete

456 evaporation of injected methanol in a short time.

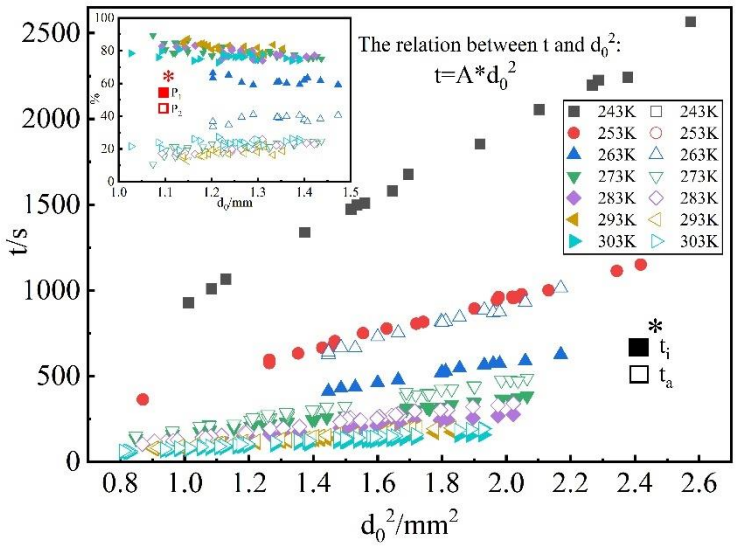

457

458 (a)

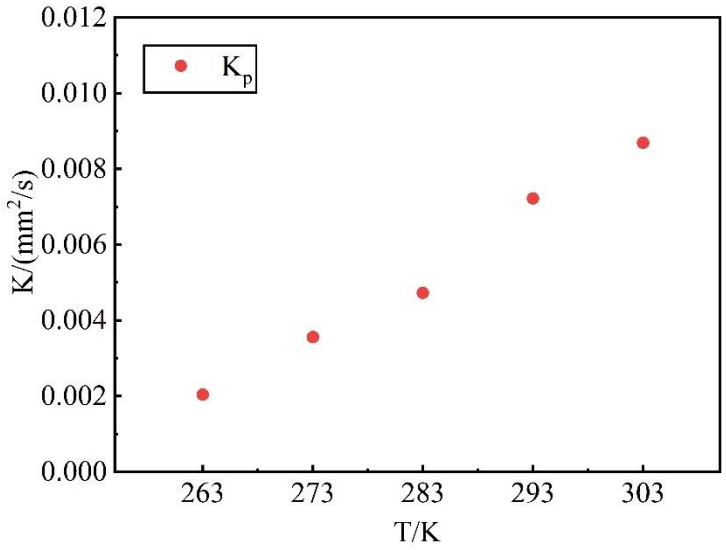

459

460 (b)

461 **Fig. 10.** (a) The ideal and actual droplet lifetimes (t_i and t_a) and the proportions of the

462 first and second stages (P_1 and P_2) under different initial droplet diameter at 243-303

463 K. (b) The effect of ambient temperature on evaporation rate constant of the pseudo

464 single component (K_p).

465

3.3 Effect of fuel temperature on methanol evaporation

Fuel temperature plays an important role on its physical properties, such as density, viscosity and surface tension [38], thus affecting the spray droplets [39]. Consequently, the effect of fuel temperature on the evaporation characteristics of methanol droplets at 273 K is investigated to reveal the underlying mechanism, which can provide guidance for practical methanol engine application. **Fig. 11** shows the temporal evolution of the normalized squared diameters and temperatures of methanol droplets with various fuel temperatures. As shown in **Fig. 11**, there is little difference in the evaporation process of droplets when methanol temperature changes. However, the relatively large difference can be found for droplet temperature curves. When the droplet is not heated, its temperature rises rapidly first, namely transient heating stage, and then rises slowly, reaching quasi-steady state, which is called equilibrium evaporation stage [40]. This occurs again in the late stage of evaporation due to the existence the second stage of methanol droplets. Adversely, the temperature of droplets with higher fuel temperature experiences first a process of rapid decline and then rising again before equilibrium evaporation. The reason may be that the hot droplets releases heat rapidly until it reaches a relatively equilibrium state with the surrounding cold environment due to their enormous temperature difference. Therefore, there is an additional transient cooling stage in the evaporation process of methanol droplets when the fuel temperature rises. And the higher fuel temperature, the longer transient cooling stage and the shorter transient heating stage. The effect of fuel temperature on the first equilibrium evaporation stage is negligible, but mainly reflects in the second equilibrium

evaporation stage. Due to the test methanol droplets is in a large space, the effect of heat transfer to the environment on the ambient temperature can be neglected, while the humidity around the droplets is changed. This means that the fuel temperature has little influence on pure methanol evaporation, but mainly affects the evaporation of methanol-water mixture.

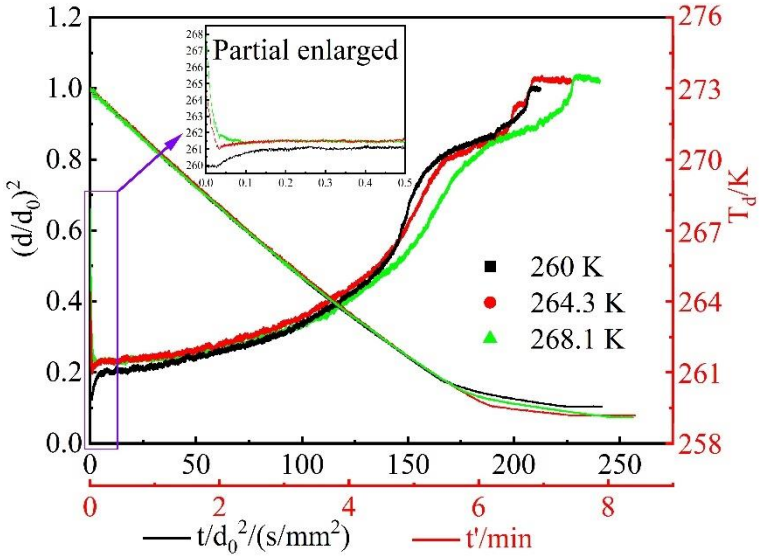

Fig. 11. Temporal evolution of the normalized squared diameters $(d/d_0)^2$ and temperatures (T_d) of methanol droplets with various fuel temperatures at ambient temperature of 273 K.

Fig. 12 illustrates the effect of fuel temperature on the average evaporation rates. As presented in **Fig. 12**, although the fuel temperature of droplets has increased by 8.5 K, the average evaporation rate of the first stage, K_1, is almost unchanged and the improved percent of K_1, P_{K1}, is around 0 % due to considerable droplet temperature rise rate in the first equilibrium evaporation stage according to **Fig. 11**. On the contrary, the average evaporation rate and its improved percent of the second stage, K_2 and P_{K2}, show remarkable fluctuation when the fuel temperature rises. It is because that the water

absorption in the second stage is influenced by the changed humidity around the methanol droplets. Ultimately, the average evaporation rate of methanol droplets, K_a, gradually decreases with the increase of fuel temperature owing to the increased proportion of the second stage shown in **Fig. 13**.

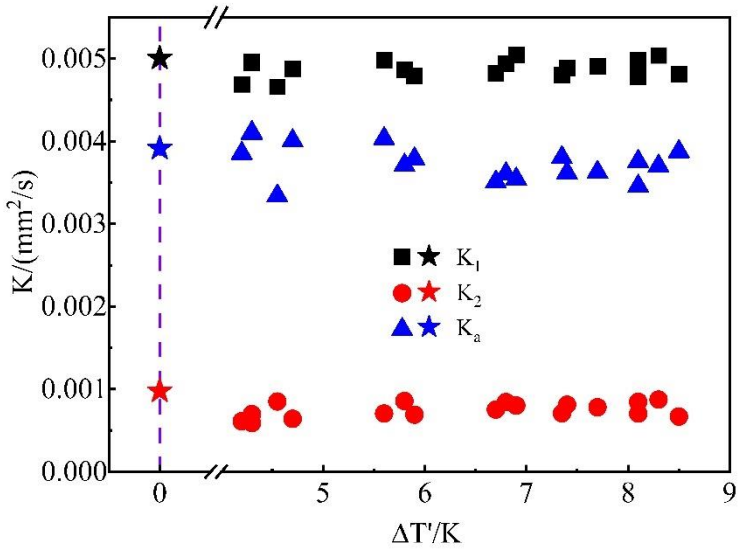

(a)

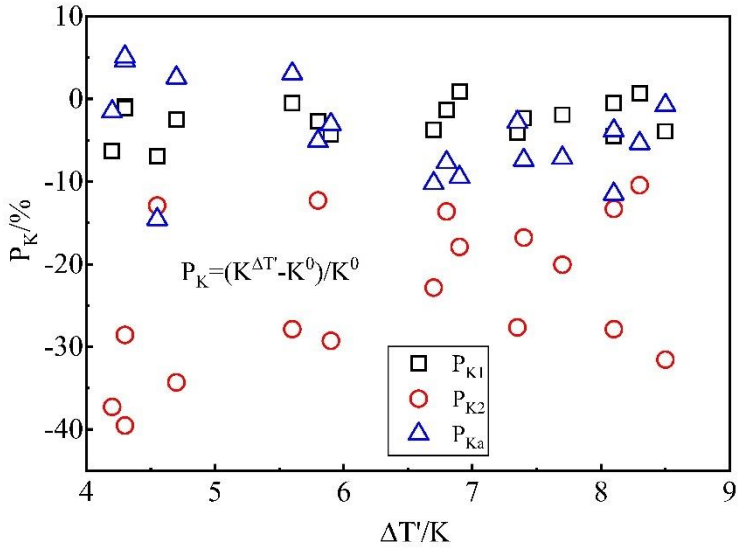

(b)

Fig. 12. Variation of the average evaporation rate of the first and second stages (K_1 and K_2) and methanol droplets (K_a) (a) and their improved percent (P_{K1}, P_{K2} and P_{Ka})

(b) with increased fuel temperature ΔT'. $K^{\Delta T'}$ represents the K after the fuel temperature increases by ΔT', K^0 represents the K under initial fuel temperature.

Fig. 13 shows the variation of ideal and actual normalized lifetimes and their increased percent with the increased fuel temperature ΔT'. It is found that the trend of ideal normalized lifetime is same as that of K_1, because the former is determined by the latter. And the increased percent of ideal normalized lifetime, $P_{\tau i}$, is also around 0 %. However, the actual normalized lifetime gradually rises with the increase of ΔT', which has a maximum improvement of 14.5 %. It is mainly due to the extension of the second stage, as shown in **Fig. 13**. According to the above discussion, improving fuel temperature cannot promote droplet evaporation in terms of its effect on evaporation rate and lifetime in this study. However, the droplet evaporation rate may be enhanced if the heat exchange between the fuel and the environment can improve the ambient temperature when the fuel temperature is high enough or the volume of environment is small. More importantly, the viscosity and surface tension of methanol can be reduced when the fuel temperature rises, then the size of spray droplets is reduced in methanol engines [41], which is significant for shortening droplet evaporation time, as discussed in section 3.2.

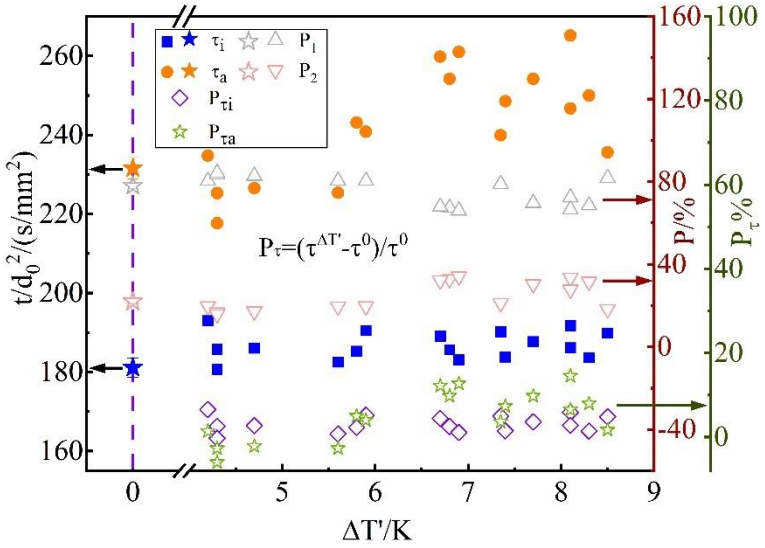

Fig. 13. Variation of the ideal and actual normalized droplet lifetimes (τ_i and τ_a) and their increased percent ($P_{\tau i}$ and $P_{\tau a}$) and the proportions of the first and second stages (P_1 and P_2) with the increased fuel temperature $\Delta T'$. $\tau^{\Delta T'}$ is the τ after the fuel temperature increases by $\Delta T'$, τ^0 is the τ under initial fuel temperature.

3.4 Effect of intake air flow velocity on methanol evaporation

It is commonly accepted that fuel droplet evaporation can be enhanced by flow. On the one hand, flow can take away the fuel vapor on the droplet surface, which promotes the diffusion of methanol molecules into the environment [42]. Furthermore, the heat transfer between the droplet and the environment is also strengthened [37]. Thus, the effect of intake air flow velocity on the improvement of methanol droplets evaporation at low temperatures is quantitively evaluated at ambient temperature of 273 K. **Fig. 14** shows temporal evolution of the normalized squared diameters and temperatures of methanol droplets at various intake air flow velocities. It is clear that the two-part feature of methanol droplets evaporation still exists, meaning that the d^2

law is not influenced by turbulence, which is consistent with the conclusion of Birouk and Fabbro [43]. And the evaporation is accelerated as expected. This promotion effect is more noticeable at low intake air flow velocity, but become weaker at higher velocity. It can be also seen from the time history of the droplet temperature that temperature rise rate of methanol droplets gradually increases with the increase of intake air flow velocity due to the enhanced heat transfer by flow.

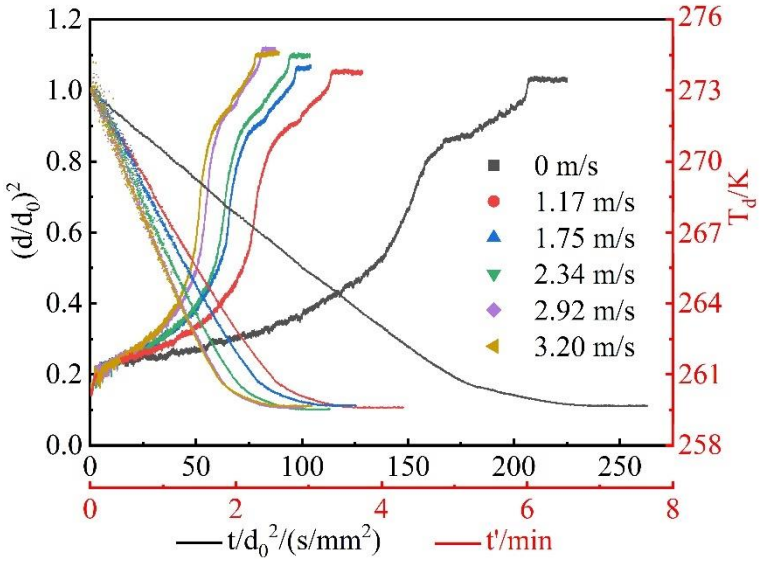

Fig. 14. Temporal evolution of the normalized squared diameters $(d/d_0)^2$ and temperatures (T_d) of methanol droplets at various intake air flow velocities and ambient temperature of 273 K.

Fig. 15 illustrates that average evaporation rates of the first and second stages and methanol droplets, K_1, K_2 and K_a, both are enhanced with the increase of intake air flow velocity. For example, K_1 is increased by 182 %, K_2 is increased by 145 % and K_a is increased by 163 % at intake air flow velocity of 2.92 m/s as compared to stationary methanol droplets, respectively. However, this enhancement is gradually weakened, because there are limits on the ability of vapor molecules to follow the fluid and the

enhancement of heat transfer [44]. The improved percent of K_1, K_2 and K_a are defined as P_{K1}, P_{K2} and P_{Ka}, respectively. It can be clearly observed that the effect of intake air flow velocity on the P_{K1}, P_{K2} and P_{Ka} is relatively small once it exceeds 3m/s. In order to quantify this weakening effect, the improvement efficiency of K_1, K_2 and K_a, η_{K1}, η_{K2} and η_{Ka}, are defined as the corresponding increased percent of the average evaporation rate divided by the intake air flow velocity, respectively, as shown in **Fig. 15**. They denote P_{K1}, P_{K2} and P_{Ka} for every 1 m/s increase in the intake air flow velocity. It is found that η_{K1} decreases from 83.28 %/(m/s) to 58.80 %/(m/s), η_{K2} decreases from 82.58 %/(m/s) to 44.52 %/(m/s) and η_{Ka} decreases from 75.90 %/(m/s) to 53.09 %/(m/s) when the intake air flow velocity increases from 1.17 m/s to 3.20 m/s, and this trend will always maintain if it continues to rise. This suggests that the benefit of strengthened intake air flow on promoting the evaporation of methanol droplets is always descending with the increase of intake air flow velocity.

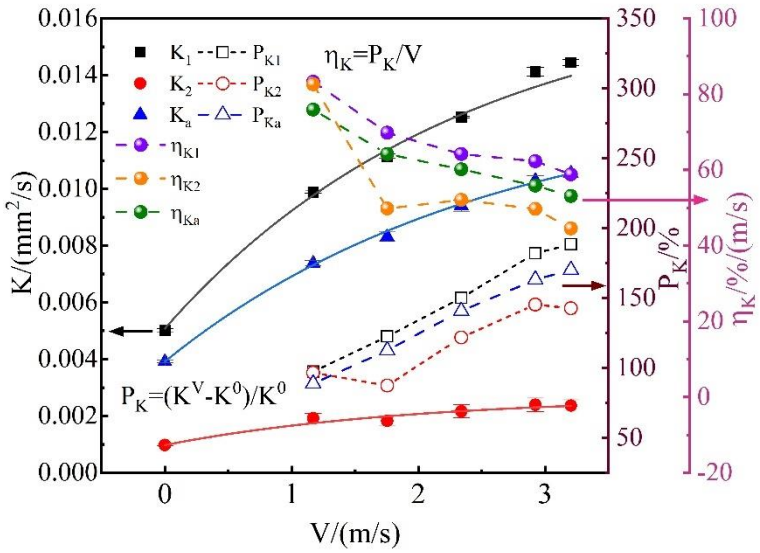

Fig. 15. Variation of the average evaporation rates of the first and second stages (K_1 and K_2) and methanol droplets (K_a) and their improved percent (P_{K1}, P_{K2} and P_{Ka}) and

improvement efficiency (η_{K1}, η_{K2} and η_{Ka}) with intake air flow velocity V. K^V is the K at intake air flow velocity of V, K^0 is the K in the quiescent state.

According to the **Fig. 16**, the proportion of the first stage, P_1, decreases and the proportion of the second stage, P_2, increases as compared to the droplets in the quiescent environment. It indicates that the flow also affects the water absorption of methanol droplets while enhancing the evaporation rate. Moreover, the effect of intake air flow on the lifetime of methanol droplets is shown in **Fig. 16**. The ideal and actual normalized lifetimes of droplets both decrease exponentially with intake air flow velocity. But their decreased percent, $P_{\tau i}$ and $P_{\tau a}$, are gradually leveling off with the increase of intake air velocity, meaning that degree of the decrease of droplet lifetime gradually decreases, e.g., the ideal and actual normalized lifetimes decrease by 50.44 % and 48.07 %, respectively, when the intake air flow velocity increases from 0 m/s to 1.17 m/s, while only 21.56 % and 21.99 %, respectively, when it increases from 1.17 m/s to 2.34 m/s. Based on the above analysis, it implies that the intake air velocity should not seemingly continue to increase when it reaches to a certain value. Considering that there is already flow in the cylinder caused by inlet stroke of methanol engines, the improvement of droplet evaporation rate caused by further increasing intake air flow velocity can be limited based on the above analysis. However, from another point of view, the flow is beneficial to spray breakup [45], thereby reducing the droplet size, which can reduce the entire evaporation time of methanol. Besides, the spatial distribution of methanol droplets can be more uniform under the action of flow. This avoids the extreme descent of temperature in the local area caused by the

concentrated evaporation of methanol to absorb a large amount of heat, then the reduction of evaporation rate of methanol droplets due to the descent of surrounding temperature can be alleviated. Therefore, high intensity turbulence is useful for improving the evaporation of methanol in the cold start process of methanol engines.

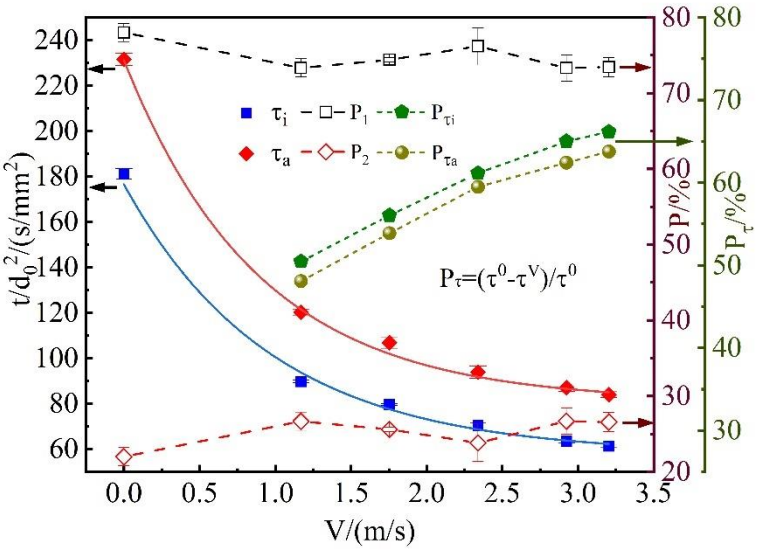

Fig. 16. Variation of the ideal and actual normalized droplet lifetimes (τ_i and τ_a), their decreased percent ($P_{\tau i}$ and $P_{\tau a}$) and the proportions of the first and second stages (P_1 and P_2) with intake air flow velocity V.

4. Conclusions

This study investigated the cold start issues of methanol engines and their improvement methods from the perspective of droplet evaporation. A wide range of fuel temperatures of 243-303 K was investigated. In particular, the low temperatures below 293 K were rarely studied in existing studies, which are of great importance for understanding the cold start issues of methanol engines and proposing effective improvement measures. The key conclusions are as follows:

(1) The evaporation process of methanol droplets with hygroscopicity consists of two stages. The first stage is the evaporation of pure methanol and the second stage is the water-dominated evaporation of methanol-water mixture, which shows noticeable difference in their evaporation rates. The droplets are evaporated by over 85% in the first stage and freeze in the second stage at temperatures below 263 K. The proportion of the second stage and the normalized droplet lifetime increase greatly when the ambient temperature is below 273 K. The empirical formulas describing the relationship between evaporation rate and ambient temperature for single-component and binary-component droplets are obtained. The average evaporation rates of methanol droplets are enhanced by increasing ambient temperature, but this promotion effect becomes weaker at higher initial ambient temperature. Increasing the ambient temperature from 243-283 to 293 K has the largest improvement efficiency of evaporation rate.

(2) The initial droplet diameter has little effect on the pure methanol evaporation, but mainly influences the evaporation of methanol-water mixture. The increase of absorbed water in methanol droplets leads to the decrease of their evaporation rates with initial droplet diameter. The proportion of the second stage increases with the increase of initial diameter and the droplet lifetime increases linearly with the square of initial diameter. The two-stage and binary-component evaporation process of methanol droplets in humid environment can be regarded as the evaporation of a pseudo single component and the same is true for other binary mixtures. The size of spray droplets should be reduced by improving injection pressure or other methods to shorten the

entire evaporation time of methanol, so that more combustible fuel/air mixture can be produced in a short time for cold start of methanol engines.

(3) The fuel temperature has little effect on the pure methanol evaporation, but mainly influences the evaporation of methanol-water mixture. There is an additional transient cooling stage before the evaporation of methanol droplets when the fuel temperature rises. With the increase of fuel temperature, the average evaporation rate of methanol droplets in humid environment decreases, while both the proportion of the second stage and the normalized droplet lifetime increase. A higher fuel temperature promotes methanol evaporation mainly through the reduced droplet size in real methanol engines when the increase of fuel temperature is insufficient.

(4) The intake air flow enhances the evaporation rate, but does not affect the two-stage feature of methanol droplet evaporation. This promotion effect is more noticeable at low intake air flow velocities and becomes weaker at higher velocity, especially when intake air flow velocity exceeds 3 m/s. With the increase of intake air flow velocity, the normalized droplet lifetime decreases exponentially, while the proportion of the second stage increases. High intensity turbulence is needed to reduce the size of spray droplets and make the descent of overall ambient temperature in the cylinder relatively small, thus improving cold start performance of methanol engines.

To sum up, multiple methods should be combined to improve the cold start performance of methanol engines efficiently. For example, to avoid a significant decrease in droplet evaporation rate caused by the massive heat absorption, the environment in the cylinder should be heated and the intake air flow velocity should be

increased. To shorten the evaporation time of methanol, the injection pressure and fuel temperature can be also increased to reduce the size of spray droplets. In the future work, molecular dynamics simulation method can be applied to investigate the behaviors of water vapor in the process of methanol evaporation and further understand the interaction between methanol and water.

Acknowledgements

The assistance from the Geely Royal Engine Components Co., Ltd is greatly appreciated.

References

[1] Huang Y, Lei C, Liu CH, Perez P, Forehead H, Kong S, et al. A review of strategies for mitigating roadside air pollution in urban street canyons. Environ Pollut 2021; 280:116971. https://doi.org/10.1016/j.envpol.2021.116971.

[2] Sacchi R, Bauer C, Cox B, Mutel C. When, where and how can the electrification of passenger cars reduce greenhouse gas emissions? Renew Sust Energ Rev 2022; 162:112475. https://doi.org/10.1016/j.rser.2022.112475.

[3] García-Olivares A, Solé J, Osychenko O. Transportation in a 100% renewable energy system. Energ Convers Manage 2018; 158:266-85. https://doi.org/10.1016/j.enconman.2017.12.053.

[4] Chen Z, Wang L, Zeng K. A comparative study on the combustion and emissions of dual-fuel engine fueled with natural gas/methanol, natural gas/ethanol, and natural gas/n-butanol. Energ Convers Manage 2019; 192:11-9. https://doi.org/10.1016/j.enconman.2019.04.011.

[5] Zhen X, Wang Y. An overview of methanol as an internal combustion engine fuel. Renew Sust Energ Rev 2015; 52:477-93. https://doi.org/10.1016/j.rser.2015.07.083.

[6] Eisavi B, Ranjbar F, Nami H, Chitsaz A. Low-carbon biomass-fueled integrated system for power, methane and methanol production. Energ Convers Manage 2022; 253:115163. https://doi.org/10.1016/j.enconman.2021.115163.

[7] Chen Z, Chen H, Wang L, Geng L, Zeng K. Parametric study on effects of excess air/fuel ratio, spark timing, and methanol injection timing on combustion characteristics and performance of natural gas/methanol dual-fuel engine at low

loads. Energ Convers Manage 2020; 210:112742. https://doi.org/10.1016/j.enconman.2020.112742.
[8] Wang Y, Long W, Tian H, Dong P, Lu M, Tang Y, et al. Research on oxidation mechanism of hydrogen/syngas-methanol and its application on engine performance prediction. Fuel 2024; 365:131211. https://doi.org/10.1016/j.fuel.2024.131211.
[9] Miganakallu N, Yang Z, Rogóż R, Kapusta ŁJ, Christensen C, Barros S, et al. Effect of water - methanol blends on engine performance at borderline knock conditions in gasoline direct injection engines. Appl Energ 2020; 264:114750. https://doi.org/10.1016/j.apenergy.2020.114750.
[10] Verhelst S, Turner JWG, Sileghem L, Vancoillie J. Methanol as a fuel for internal combustion engines. Prog Energ Combust 2019; 70:43-88. https://doi.org/10.1016/j.pecs.2018.10.001.
[11] Gong C, Yi L, Zhang Z, Sun J, Liu F. Assessment of ultra-lean burn characteristics for a stratified-charge direct-injection spark-ignition methanol engine under different high compression ratios. Appl Energ 2020; 261:114478. https://doi.org/10.1016/j.apenergy.2019.114478.
[12] Chen Z, Wang L, Yuan X, Duan Q, Yang B, Zeng K. Experimental investigation on performance and combustion characteristics of spark-ignition dual-fuel engine fueled with methanol/natural gas. Appl Therm Eng 2019; 150:164-74. https://doi.org/10.1016/j.applthermaleng.2018.12.168.
[13] Wang B, Wang H, Yang C, Hu D, Duan B, Wang Y. Effect of different ammonia/methanol ratios on engine combustion and emission performance. Appl Therm Eng 2024; 236:121519. https://doi.org/10.1016/j.applthermaleng.2023.121519.
[14] Chen Z, Wang L, Zhang Q, Zhang X, Yang B, Zeng K. Effects of spark timing and methanol addition on combustion characteristics and emissions of dual-fuel engine fuelled with natural gas and methanol under lean-burn condition. Energ Convers Manage 2019; 181:519-27. https://doi.org/10.1016/j.enconman.2018.12.040.
[15] Xu L, Treacy M, Zhang Y, Aziz A, Tuner M, Bai X-S. Comparison of efficiency and emission characteristics in a direct-injection compression ignition engine fuelled with iso-octane and methanol under low temperature combustion conditions. Appl Energ 2022; 312:118714. https://doi.org/10.1016/j.apenergy.2022.118714.
[16] Çelik MB, Özdalyan B, Alkan F. The use of pure methanol as fuel at high compression ratio in a single cylinder gasoline engine. Fuel 2011; 90(4):1591-8. https://doi.org/10.1016/j.fuel.2010.10.035.
[17] Balki MK, Sayin C. The effect of compression ratio on the performance, emissions and combustion of an SI (spark ignition) engine fueled with pure ethanol, methanol and unleaded gasoline. Energy 2014; 71:194-201. https://doi.org/10.1016/j.energy.2014.04.074.
[18] Zhu Z, Mu Z, Wei Y, Du R, Liu S. Experimental evaluation of performance of heavy-duty SI pure methanol engine with EGR. Fuel 2022; 325:124948.

https://doi.org/10.1016/j.fuel.2022.124948.
[19] Li J, Gong C, Su Y, Dou H, Liu X. Effect of Preheating on Firing Behavior of a Spark-Ignition Methanol-Fueled Engine during Cold Start. Energ Fuel 2009; 23(11):5394-400. https://doi.org/10.1021/ef900569a.
[20] Gao Y, Wei M, Yan F, Chen L, Li G, Feng L. Effects of cavitation flow and stagnant bubbles on the initial temporal evolution of diesel spray. Experimental Thermal Fluid Science 2017; 87:69-79. https://doi.org/10.1016/j.expthermflusci.2017.04.029.
[21] Pinheiro AP, Vedovoto JM, da Silveira Neto A, van Wachem BGM. Ethanol droplet evaporation: Effects of ambient temperature, pressure and fuel vapor concentration. Int J Heat Mass Tran 2019; 143:118472. https://doi.org/10.1016/j.ijheatmasstransfer.2019.118472.
[22] Yuan B, Wang Z, Cao J, Huang Y, Shen Y, Song Z, et al. Mixture formation characteristics and feasibility of methanol as an alternative fuel for gasoline in port fuel injection engines: Droplet evaporation and spray visualization. Energ Convers Manage 2023; 283:116956. https://doi.org/10.1016/j.enconman.2023.116956.
[23] Wang F, Yao J, Yang S, Liu R, Jin J. A new stationary droplet evaporation model and its validation. Chinese Journal of Aeronautics 2017; 30(4):1407-16. https://doi.org/10.1016/j.cja.2017.06.012.
[24] Law C, Xiong T, Wang C. Alcohol droplet vaporization in humid air. Int J Heat Mass Tran 1987; 30(7):1435-43. https://doi.org/10.1016/0017-9310(87)90175-x.
[25] Hegseth JJ, Rashidnia N, Chai A. Natural convection in droplet evaporation. Phys Rev E 1996; 54(2):1640. https://doi.org/10.1103/PhysRevE.54.1640.
[26] Kosasih EA, Agung I, Siahaan AT, Prasetyo D. Heat and mass transfer of ethanol and methanol droplets with temperature and air flow rates variations. *AIP Conference Proceedings*. 2062. AIP Publishing; 2019.
[27] Rehman HL-u, Weiss J, Seers P. Effect of heat conduction on droplet life time and evaporation rate under forced convection at low temperatures. Exp Therm Fluid Sci 2016; 72:59-66. https://doi.org/10.1016/j.expthermflusci.2015.10.030.
[28] Moffat R. Describing the uncertainties in experimental results. Exp Therm Fluid Sci 1988; 1(1):3-17. https://doi.org/10.1016/0894-1777(88)90043-x.
[29] Zhang Y, Huang R, Xu S, Huang Y, Huang S, Ma Y, et al. The effect of different n-butanol-fatty acid methyl esters (FAME) blends on puffing characteristics. Fuel 2017; 208:30-40. https://doi.org/10.1016/j.fuel.2017.07.001.
[30] Han K, Liu Y, Wang C, Tian J, Song Z, Lin Q, et al. Experimental study on the evaporation characteristics of biodiesel-ABE blended droplets. Energy 2021; 236:121453. https://doi.org/10.1016/j.energy.2021.121453.
[31] Morin C, Chauveau C, Gökalp I. Droplet vaporisation characteristics of vegetable oil derived biofuels at high temperatures. Exp Therm Fluid Sci 2000; 21(1-3):41-50. https://doi.org/10.1016/S0894-1777(99)00052-7.
[32] Zhang Y, Huang R, Wang Z, Xu S, Huang S, Ma Y. Experimental study on puffing characteristics of biodiesel-butanol droplet. Fuel 2017; 191:454-62.

https://doi.org/10.1016/j.fuel.2016.11.103.
[33] Lee A, Law CK. An experimental investigation on the vaporization and combustion of methanol and ethanol droplets. Combust Sci Technol 1992; 86(1-6):253-65. https://doi.org/10.1080/00102209208947198.
[34] Wakisaka A, Komatsu S, Usui Y. Solute-solvent and solvent-solvent interactions evaluated through clusters isolated from solutions: Preferential solvation in water-alcohol mixtures. J Mol Liq 2001; 90:175-84. https://doi.org/https://doi.org/10.1016/S0167-7322(01)00120-9.
[35] Park SH, Kim HJ, Lee CS. Macroscopic spray characteristics and breakup performance of dimethyl ether (DME) fuel at high fuel temperatures and ambient conditions. Fuel 2010; 89(10):3001-11. https://doi.org/10.1016/j.fuel.2010.05.002.
[36] Verwey C, Birouk M. Experimental investigation of the effect of natural convection on the evaporation characteristics of small fuel droplets at moderately elevated temperature and pressure. Int J Heat Mass Tran 2018; 118:1046-55. https://doi.org/10.1016/j.ijheatmasstransfer.2017.11.038.
[37] Verwey C, Birouk M. Experimental investigation of the effect of droplet size on the vaporization process in ambient turbulence. Combust Flame 2017; 182:288-97. https://doi.org/10.1016/j.combustflame.2017.04.027.
[38] Park Y, Hwang J, Bae C, Kim K, Lee J, Pyo S. Effects of diesel fuel temperature on fuel flow and spray characteristics. Fuel 2015; 162:1-7. https://doi.org/10.1016/j.fuel.2015.09.008.
[39] Shin J, Kim D, Seo J, Park S. Effects of the physical properties of fuel on spray characteristics from a gas turbine nozzle. Energy 2020; 205:118090. https://doi.org/10.1016/j.energy.2020.118090.
[40] Xi X, Liu H, Cai C, Jia M, Ma X. Analytical and experimental study on boiling vaporization and multi-mode breakup of binary fuel droplet. Int J Heat Mass Tran 2021; 165:120620. https://doi.org/10.1016/j.ijheatmasstransfer.2020.120620.
[41] Chen Z, Yao A, Yao C, Yin Z, Xu H, Geng P, et al. Effect of fuel temperature on the methanol spray and nozzle internal flow. Appl Therm Eng 2017; 114:673-84. https://doi.org/10.1016/j.applthermaleng.2016.12.025.
[42] Patel U, Sahu S. Effect of air turbulence and fuel composition on bi-component droplet evaporation. Int J Heat Mass Tran 2019; 141:757-68. https://doi.org/10.1016/j.ijheatmasstransfer.2019.06.067.
[43] Birouk M, Fabbro SC. Droplet evaporation in a turbulent atmosphere at elevated pressure – Experimental data. Proceedings of the Combustion Institute 2013; 34(1):1577-84. https://doi.org/10.1016/j.proci.2012.05.092.
[44] Wang Z, Yuan B, Huang Y, Cao J, Wang Y, Cheng X. Progress in experimental investigations on evaporation characteristics of a fuel droplet. Fuel Process Technol 2022; 231:107243. https://doi.org/10.1016/j.fuproc.2022.107243.
[45] Si Z, Ashida Y, Shimasaki N, Nishida K, Ogata Y. Effect of cross-flow on spray structure, droplet diameter and velocity of impinging spray. Fuel 2018; 234:592-603. https://doi.org/10.1016/j.fuel.2018.07.061.